Measurement Setup and Modeling Approach for the Deformation of Robot Bodies During Machining

L. Gründel(✉), J. Schäfer, S. Storms, and C. Brecher

Laboratory for Machine Tools and Production Engineering (WZL) of RWTH Aachen University, Aachen, Germany
l.gruendel@wzl.rwth-aachen.de

Abstract. Conventional industrial robots (IR) represent a cost-effective machining alternative for large components. However, due to the serial kinematics and the resulting high tool deflections, they usually lack precision. Model-based simulation and control methods are used to increase the accuracy of IR regarding both planning and the process itself. The majority of the applied models include the compliances of the gears and bearings but neglect the deformations of the manipulator bodies. This paper introduces an approach to directly measure and evaluate the deformation of robot bodies in the presence of process forces. The measurement setup contains multiple Integral Deformation Sensors (IDS), which provide the change of length due to deformations of the respective body. Subsequently, the measurements are fed to a beam model (BM), which calculates the body's 3D Cartesian deflections. The presented approach is validated by static tensile tests on a conventional six-degree-of-freedom (DOF) robot manipulator.

Keywords: Robot machining · Deformation measurements · Beam theory

1 Introduction

Especially for small and medium-sized enterprises IR represent a lower investment risk compared to conventional machine tools. Furthermore, they offer flexibility in both positioning and applications and operate in wide workspaces. Therefore, robot machining has become more and more relevant for research and industry [1]. Nonetheless, IR exhibit a significantly higher compliance at the Tool Center Point (TCP) compared to machine tools [2] due to:

- non-preloaded drivetrains,
- space-optimized gearboxes with lower stiffness and larger backlash,
- more compliant components as bearings and robot bodies and
- an unfavorable mass distribution due to the serial structure.

The higher compliance at the TCP results in lower machining quality and an increasing tendency to chatter, which negatively affects the process stability [2].

M. Liewald et al. (Eds.): WGP 2022, LNPE, pp. 324–334, 2023.
https://doi.org/10.1007/978-3-031-18318-8_34

In addition to dedicated robot designs [3] or optimizations such as direct encoders at the joints [4], various model-based compensation approaches were developed over the recent years (cf. *Chapter 2*). The key element of any model-based compensation approach is the compliance model of the IR, which simulates the robot deflections due to process forces at the TCP. Since the main cause for deflections at the TCP is usually attributed to the stiffness of drivetrains and bearings, they are widely investigated metrologically and integrated in existing compensation approaches. The behavior of the bodies, on the other hand, is typically cumulated with the bearings or assumed to be ideally rigid [5, 6]. In addition, common measurement setups tend to identify the different stiffness parameters of the components together, which leads to errors.

The main contribution of this paper is the presentation of a measurement setup and modeling approach, which allows the decoupled measurement and simulation of the 3D deformations of beam-like robot bodies. Furthermore, the swing deformation is integrated into the compliance model via an extension of the Virtual Joint Method (cf. *Chapter 2*). The setup, containing IDS as described in [7] and [8], is validated and evaluated based on experiments on a conventional IR.

The paper is structured as follows: First, we discuss the state of the art regarding compensation, modeling and stiffness parameter identification approaches in Chapter 2. Then the BM is described in Chapter 3. Afterwards, the measurement setup is presented (cf. Chapter 3), followed by a validation and evaluation of the approach in Chapter 5. Finally, the results are summarized and an outlook on further research activities is given in Chapter 6.

2 State of the Art

In [9] a model-based process planning approach for robot machining is presented, which allows the process planner to avoid critical cutting parameters. The method is based on a static stiffness model. SCHNOES and ZAEH extend the stiffness model with a process force model. Hereby, the optimal workpiece placement and process parameters are determined and compensation offsets are calculated [10]. In [11] the authors present a model-based feed-forward control to compensate force-induced deviations at the TCP. Here, the model is based on the equations of motion derived from the Lagrangian equation coupled with a stiffness model. klimchik et al. Apply both, online and offline compensation, in order to increase the robots accuracy during machining [12]. The experiments with a KUKA KR270 showed a decrease of the maximum deviation by more than 90%.

In general, the stiffness respectively compliance models can be divided into three main groups [13].

- Finite Element Analysis (FEA)
- Structural Matrix Analysis (SMA)
- Virtual Joint Method (VJM).

FEA, as the most precise method, is mostly used in the final design phase of the IR, since the mesh fitting requires a lot of computation power. SMA follows the concept of FEA, but uses larger elements rather than finite elements. For example, the arm parts

are represented as flexible 3D beams, which significantly reduces the computational effort. VJM is the most widely used approach for disturbance compensation in robot-based machining processes. It is based on the extension of the rigid multibody model by virtual joints describing the elastic deformations of the links, joints and actuators [13, 14].

Although the compensation of the static displacements is given a high priority in all the approaches mentioned above, the stiffness of the bodies is usually neglected. The models mostly include torsional and tilting stiffnesses of the joints, which can be identified in static tensile tests [5, 6]. Here, the force is applied via a pneumatic cylinder or a tension rod and the displacement is measured tactilely or via laser trackers. While these tests allow a proper excitation of the compliance parameters, the routine can only measure all parameters at once and therefore implies coupling errors between axes. Besides individual approaches such as [15], there are only a few methods that identify joint stiffnesses in a decoupled manner.

In [16] the beam-like robot bodies—the so-called swing (S) between axis 2 and 3 and the arm (A) between axis 3 and the wrist—are approximated with two ideal rigid bars and three torsion springs halfway along the body, respectively. In contrast to the widespread assumption that the robot bodies are negligible because they do not affect the total compliance of the IR, measurements in [16] show that the beam-like bodies (S and A, cf. Table 1) exhibit compliances in the same order of magnitude as the other components. RÖSCH identified the shown values with a static tensile test as described above using 3D-laser-scanning-vibrometry. The described measurement setup offers the identification of the bodies but also relies on coupled measurements of all components, which lead to coupling effects and therefore errors.

Table 1. Identified stiffness parameters of a KUKA KR240 in [Nm/rad], acc. to [16]

Joint	1	2	S	3	A	4	5	6
Bearing c_α	1,4e7	1,5e7	7,7e6	4,1e6	3,6e6	3,9e6	3,7e6	3,7e6
Bearing c_β	1,4e7	1,5e7	7,0e6	4,1e6	2,9e6	3,9e6	3,7e6	3,7e6
Gear c_γ	5,4e6	8,7e6	1,1e7	5,2e6	1,7e7	1,0e6	1,2e6	3,8e8

Summarizing the modeling and parameter identification approaches from the literature, there is no separate method for identification and validation of the link's stiffnesses. In addition, the impact of link deflections for any loading case was only evaluated by coupled measurements of the whole IR rather than for separate measurements at the links.

One method for separate measurements are IDS. In the field of machine tools, they are mainly used to measure thermal deformations as in [7] and [8]. The measuring principle of an IDS relies on a reference rod that is mounted on the surface of the machine structure (cf. Fig. 1). By supporting this rod with a fixed and a loose bearing, the rod can move axially in the loose bearing when the structure is deformed under an external load. A length gauge with a tactile measuring tip is attached to the structure on

the side of the loose bearing to measure the displacement of the rod. In this way, the translational deformation of the structure between the attachment points of the IDS can be captured along the rod.

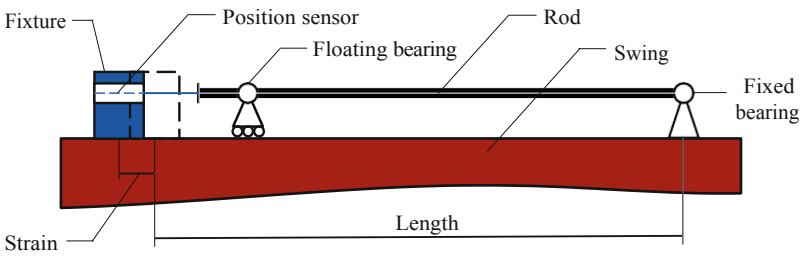

Fig. 1. Structure of an IDS

In the following chapter, the modeling approach is explained, followed by the experiments, which will present the usage of IDS to identify stiffness parameters.

3 Compliance Modeling

With the strain or contraction along its length each IDS provides a one-dimensional information about the deformation field of the machine structure. The detection of complex deformations due to tension, compression, bending, shear and torsion requires the installation of several IDS. In order to precisely calculate the deformation field of the structure based on measured IDS data, a suitable mechanical deformation model and a sufficient number of well-positioned sensors are necessary. The expected deformational behavior and the demands on accuracy determine the choice of the model. The required number of sensors depends on the model.

Since the swing can be considered as a beam-shaped component, a beam model is chosen to calculate the deformation field. Comparing bending stiffness and shear stiffness, the swing can be modeled based on the Euler-Bernoulli theory acc. to [17] (cf. Fig. 2). Therefore, the three-dimensional deformation field can be described using the deformation vector u acc. to (1).

$$\boldsymbol{u}(\boldsymbol{x}) = \begin{bmatrix} u_1 \\ u_2 \\ u_3 \\ \varphi_1 \\ \varphi_2 \\ \varphi_3 \end{bmatrix} = \begin{bmatrix} \overline{u}_1(x_1) - x_2 \cdot \varphi_3(x_1) + x_3 \cdot \varphi_2(x_1) \\ \overline{u}_2(x_1) \\ \overline{u}_3(x_1) \\ 0 \\ \varphi_2(x_1) \\ \varphi_3(x_1) \end{bmatrix}, \quad \text{with} \tag{1}$$

$$\varphi_3(x_1) = \overline{u}_2'(x_1) = \frac{\partial \overline{u}_2(x_1)}{\partial x_1} \tag{2}$$

$$\varphi_2(x_1) = -\overline{u}_3'(x_1) = -\frac{\partial \overline{u}_3(x_1)}{\partial x_1}. \tag{3}$$

where u_1, u_2 and u_3 describe the translational and φ_1, φ_2 and φ_3 describe the rotational displacements in the coordinate system corresponding to Fig. 3. $\overline{u}_1$ represents a longitudinal shift due to tension or compression, while $\overline{u}_2$ and $\overline{u}_3$ are transverse shifts because of bending. While φ_1 describes a rotation around the longitudinal axis due to torsion, φ_2 and φ_3 represent rotations around the respective transverse axis due to bending.

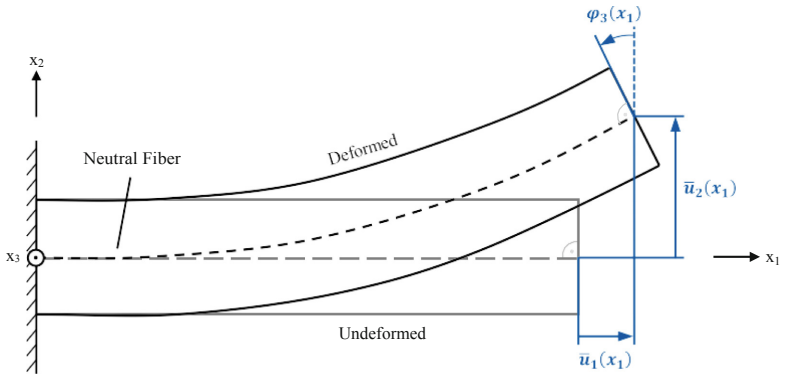

Fig. 2. Euler-Bernoulli beam model

The extension of the deformation field in (1) by deformations due to torsion allows a more precise prediction of the deformation behavior. The swing has a thin-walled closed cross-section. With this cross-sectional profile, a rotation around its longitudinal axis (torsion) and a translational displacement of the cross-section along the longitudinal axis (warping) occur as a result of torsional load. The swing can be modeled as a cantilever beam, with a fixed clamping at joint 2. Thus, torsion and warping are prevented at this point. At the free end, however, both deformations can occur unhindered. In order to consider torsion and warping in the deformation vector it is necessary to integrate additional terms. For this purpose, the kinematic assumptions for the deformation field within the Saint-Venant torsion theory can be used [18]. The extended deformation vector u_{est} reads:

$$\boldsymbol{u}_{\text{ext}}(\boldsymbol{x}) = \begin{bmatrix} \overline{u}_1(x_1) - x_2 \cdot \varphi_3(x_1) + x_3 \cdot \varphi_2(x_1) + \Psi(x_2, x_3) \cdot \kappa_1 \\ \overline{u}_2(x_1) - x_3 \cdot \varphi_1(x_1) \\ \overline{u}_3(x_1) + x_2 \cdot \varphi_1(x_1) \\ \varphi_1(x_1) \\ \varphi_2(x_1) \\ \varphi_3(x_1) \end{bmatrix}, \quad \text{with} \tag{4}$$

$$\kappa_1(x_1) = \varphi_1'(x_1) = \frac{\partial \varphi_1(x_1)}{\partial x_1}. \tag{5}$$

where Ψ is the warping function and κ_1 is the relative twist following (5), which is assumed to be constant. The coordinate system CF_{BM}, which the deformation vector of the swing refers to, is aligned with the averaged neutral fiber (ANF) in the middle

sector of the swing as shown in Fig. 3. In order to integrate the swing deformation into the compliance model, the deformation is calculated at the target point, which marks the connection between swing and arm (cf. Fig. 3).

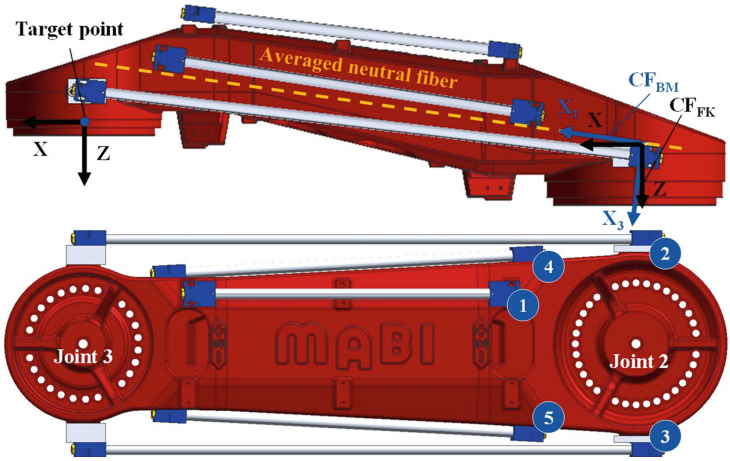

Fig. 3. Positioning of the IDS on the swing and coordinate system definition

The deformation behavior of the swing is determined using the extended Euler-Bernoulli BM in (4). Therefore, the four independent deformational DOF $\overline{u}_1$, $\overline{u}_2$, $\overline{u}_3$ and φ_1 are described as functions of the measured IDS data. For each of the mentioned deformational DOF a polynomial of third order is set up acc. to [8]. Subsequently, the derivations of these polynomials φ_2, φ_3 and κ_1 can be calculated acc. to (2), (3) and (5), as soon as the coefficients of the polynomials are identified. In order to calculate the coefficients of the polynomials mechanical boundary conditions are required. These are derived from the assumptions for cantilever beams and the IDS data. Since each IDS is aligned along the ANF, the relationship between the IDS_n data $_{\mathrm{n}}$ and the translational deformation u_1 in (6) applies,

$$IDS_n = \int_{x_{1B,IDS_n}}^{x_{1E,IDS_n}} \frac{\partial u_1(\boldsymbol{x})}{\partial x_1} dx_1 \tag{6}$$

where $x_{1B,IDSn}$ and $x_{1E,IDSn}$ define the attachment points of an IDS. Hence, for the four independent deformational DOF four IDS are required, while a fifth sensor is installed to provide redundant information. Figure 3 shows the positioning of the deployed IDS. Having identified the coefficients, the polynomials $\overline{u}_1$, $\overline{u}_2$, $\overline{u}_3$ and φ_1 and their derivations φ_2, φ_3 and κ_1 can be determined. Subsequently, the deformation vector for the target point is calculated with the respective IDS data following (4).

The deformations of the swing at the defined target point can be interpreted as a translational and rotational displacement of the coordinate system at joint 3. First, the translational displacement is carried out. Therefore, the deformations calculated in

CF_{BM} are transformed into CF_{FK} (cf. Fig. 3). The body-fixed coordinate system CF_{FK} is aligned to the coordinate system at joint 3. Hence, their orientation coincides for any axis configuration and loading case. Extending the forward kinematics of the robot by the additional transformations, the deformation of the swing is integrated into the compliance model. Hence, the robot deflections at the TCP due to the compliance of the swing can be simulated. The validity of the measurement setup and the modeling approach is evaluated in the following chapters.

4 Experiments

The experiments are carried out on the six DOF IR MAX100 by MABI Robotic AG controlled by the Numerical Control (NC) Sinumerik 840d sl by Siemens AG (cf. Fig. 4). As already mentioned in Chapter 3, there are five IDS mounted on the swing of the IR. The force is applied with a Load Displacement Measuring Device (LDMD). The device applies compressive and tensile force curves at the TCP and allows the simultaneous measurement of the displacement and the force in the respective direction. In the following chapters, the applied forces are always defined in the base coordinate system shown in Fig. 4. The change of length within the IDS is measured with an Acanto position sensor by HEIDENHAIN GmbH.

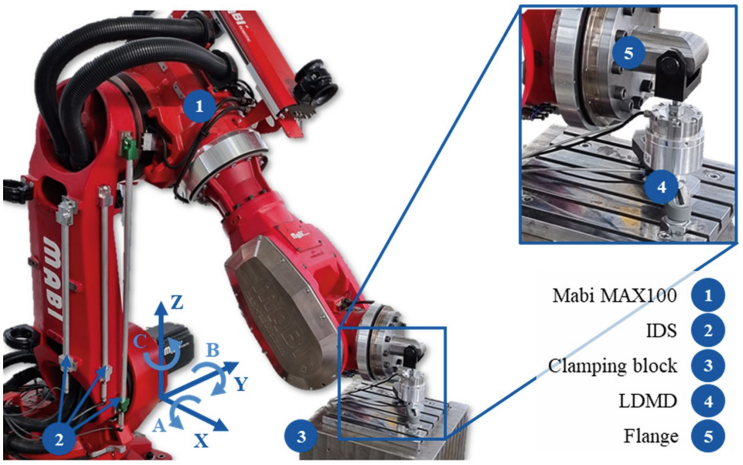

Fig. 4. Measurement setup

The IDS data is measured with a standard Industrial PC (IPC) by Beckhoff Automation GmbH & Co. KG, the IR configuration with the NC and the force and displacement with a National Instruments PC. During the measurements the data is pushed to a time series database (TimescaleDB) and is synchronized in time.

For the validation of the measurement setup and the BM and for the evaluation of the swing's influence on the total compliance of the IR eight measurement configurations were chosen (cf. Table 2). The poses cover the workspace in front of the workspace and

enable different force directions. In the following section the approaches are validated and evaluated.

Table 2. Measurement poses

Pose No.	Axis No.						Force direction
	1	2	3	4	5	6	
1	−21	33	40	22	−73	−96	−Y
2	−2	11	69	1	−56	0	−X
3	−1	17	36	1	−55	0	Z
4	17	54	36	−17	−94	90	Y
5	−3	33	35	−2	20	93	Y
6	−26	5	53	2	31	24	−X
7	−20	16	15	0	59	20	Z
8	−34	32	11	0	47	124	−Y

5 Validation and Evaluation

First, the validity of the measurement setup is checked by superimposing the force data with the respective IDS data. In Fig. 5, the force and IDS data is shown for pose 1, where the force is applied in –Y direction of the base coordinate system. The force curve shows that the tensile area was not optimally reached. This behavior was also observed in other measurement poses and is attributed to the difficult-to-handle zeroing of the LDMD.

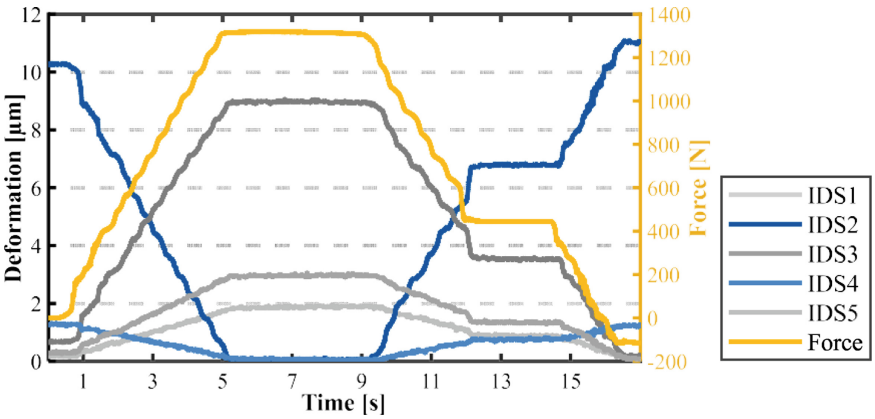

Fig. 5. Validation of the measurement setup with the respective deformations of the IDS according to the force applied in –Y direction in pose 1

Furthermore, the waviness of the force ramp as it rises and falls is attributed to friction in the LDMD housing. Nevertheless, the shown plots suggest a strong correlation between the force applied at the TCP and the measured deformations. Even the mentioned waviness is reproduced in the IDS data. As the IDS pairs 2, 3 and 4, 5 are positioned on opposite sides of the swing, the respective data shows antiproportional behavior. In addition, the shorter the IDS rod is, the less deformation is measured (cf. Fig. 3). Summing up, the measurement setup allows to excite the swing's deformations in the expected manner.

In Fig. 6, the resulting Cartesian displacements calculated with the presented BM are validated for pose 1. The data refer to coordinate system CF_{FK}, as shown in Fig. 3. As expected, the translational displacements in Z are the highest as the force is applied in the same direction at the TCP. The relatively small displacement in A suggests that the swing is stiffer in torsional direction. The bending of B is higher than in C direction, which seems intuitively correct after considering the swing model (cf. Fig. 3).

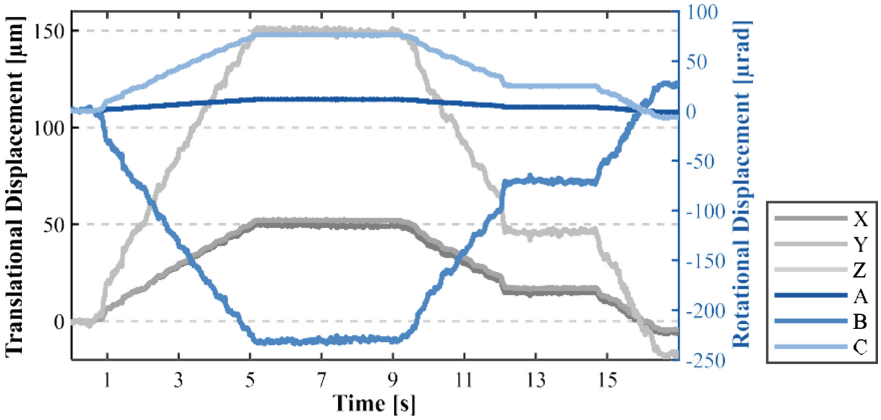

Fig. 6. Calculation of the Cartesian Displacements of the swing with the beam model in pose 1

Finally, the models for the total compliance at the TCP with and without the swing deformation are compared with the measured displacements. In Fig. 7 this comparison is shown exemplary for poses 1, 2, 6 and 8. As expected the overall compliance is higher in Y direction. Apart from a force-proportional offset, the simulated data shows a strong correlation with the measured displacements. The marginally improved simulation of the displacement with the integrated swing deformation suggests that the swing was successfully integrated. Nevertheless the influence of the swing is comparably low to the rest of the deformed components.

Summing up, the measurement setup proved to be a valid way to investigate the behavior of the swing separately. However, in order to make a sufficiently validated statement about the influence of the swing on the total compliance of the IR, further experiments should be carried out.

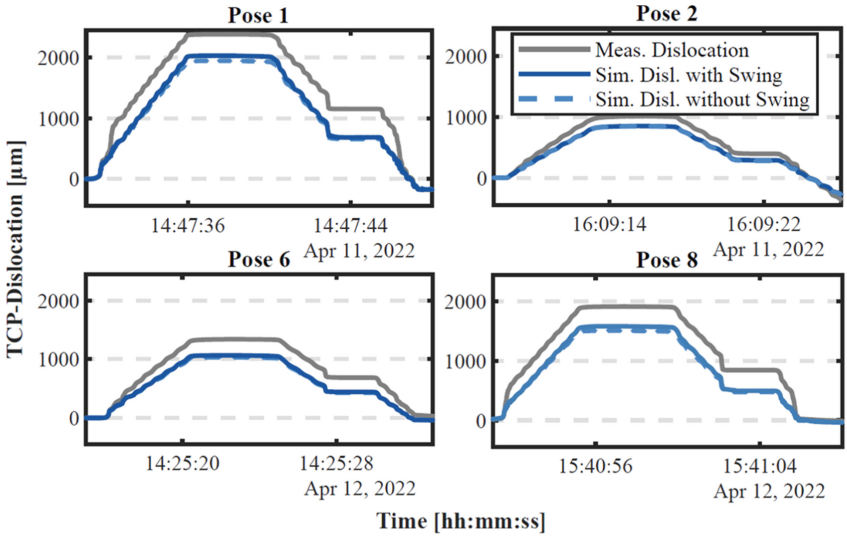

Fig. 7. Comparison of the measured and simulated dislocation of the TCP with and without the swing deformations included

6 Summary and Outlook

Due to an increasing relevance of conventional IR for machining tasks, model-based compensation approaches were developed during the past years. In contrast to the drivetrains and bearings the deformation of the robot bodies is often neglected and therefore not compensated. So far, there is no measurement setup to evaluate the body's influence on the total compliance separately.

Therefore, this paper presents both a measurement setup and a modeling approach for the beam-like bodies of an IR. The model is derived following the Euler-Bernoulli beam theory and the measurements are carried out with five IDS and a LDMD to apply forces and measure deflections at the TCP. The approach is validated on the swing of a conventional six DOF IR. The results show the intendent behavior of the measured deformation according to the applied forces. In addition, the BM shows valid results for the Cartesian deformation and the simulated total compliance at the TCP is marginally improved by integrating the swing. Nevertheless, further experiments will be carried out for a final evaluation.

Apart from smaller adjustments to the measurement setup and further stiffness experiments, the 6×6 compliance matrix of the swing is required in order to predict the deformation related to the applied force without IDS data. After a final evaluation of the developed prediction model, the compensation approach will be integrated as a feed-forward control.

Acknowledgements. The IGF-project 21926 N/2 (RoSiKo) of the research association FVP (Forschungsver-einigung Programmiersprachen für Fertigungseinrichtungen e.V.) was supported via the AiF within the funding program "Industrielle Gemeinschaftsforschung und—entwicklung

(IGF)" by the Federal Ministry of Economic Affairs and Climate Action (BMWK) due to a decision of the German Parliament. Furthermore, we gratefully acknowledge the support of the MABI Robotic AG and the support by D. Tipura and D. Vogel.

References

1. Verl, A., Valente, A., Melkote, S., et al.: Robots in machining. CIRP Ann. **68**, 799–822 (2019). https://doi.org/10.1016/j.cirp.2019.05.009
2. Pan, Z., Zhang, H., Zhu, Z., et al.: Chatter analysis of robotic machining process. J. Mater. Process. Technol. **173**, 301–309 (2006). https://doi.org/10.1016/j.jmatprotec.2005.11.033
3. Denkena, B., Bergmann, B., Lepper, T.: Design and optimization of a machining robot. Proc. Manuf. **14**, 89–96 (2017). https://doi.org/10.1016/j.promfg.2017.11.010
4. Möller, C., Schmidt, H.C., Koch, P., et al.: Machining of large scaled CFRP-Parts with mobile CNC-based robotic system in aerospace industry. Proc. Manuf. **14**, 17–29 (2017). https://doi.org/10.1016/j.promfg.2017.11.003
5. Cordes, M., Hintze, W.: Offline simulation of path deviation due to joint compliance and hysteresis for robot machining. Int. J. Adv. Manuf. Technol. **90**(1–4), 1075–1083 (2016). https://doi.org/10.1007/s00170-016-9461-z
6. Dumas, C., Caro, S., Cherif, M., et al.: Joint stiffness identification of industrial serial robots. Robotica **30**, 649–659 (2011). https://doi.org/10.1017/S0263574711000932
7. Baum, C., Brecher, C., Klatte, M., et al.: Thermally induced volumetric error compensation by means of integral deformation sensors. Proc. CIRP **72**, 1148–1153 (2018). https://doi.org/10.1016/j.procir.2018.03.045
8. Brecher, C., Klatte, M., Lee, T.H., et al.: Metrological analysis of a mechatronic system based on novel deformation sensors for thermal issues in machine tools. Proc. CIRP **77**, 517–520 (2018). https://doi.org/10.1016/j.procir.2018.08.245
9. Lienenlüke, L., Gründel, L., Storms, S. et al.: Model-based process planning for milling operations using industrial robots. In: 2018 3rd International Conference on Control and Robotics Engineering (ICCRE), pp 37–44. IEEE (2018)
10. Schnoes, F., Zaeh, M.F.: Model-based planning of machining operations for industrial robots. Procedia CIRP **82**, 497–502 (2019). https://doi.org/10.1016/j.procir.2019.04.331
11. Gründel, L., Lienenlüke, L., Storms, S., et al.: Robot-based milling operation. Machine learning algorithm for a model-based feed-forward torque control. WT Werkstattstechnik **109**, 352–357 (2019)
12. Klimchik, A., Bondarenko, D., Pashkevich, A. et al.: Compensation of tool deflection in robotic-based milling (2012)
13. Pashkevich, A., Klimchik, A., Chablat, D.: Enhanced stiffness modeling of manipulators with passive joints. Mech. Mach. Theory **46**, 662–679 (2011). https://doi.org/10.1016/j.mechmachtheory.2010.12.008
14. Klimchik, A., Wu, Y., Caro, S., Furet, B., Pashkevich, A.: Accuracy Improvement of robot-based milling using an enhanced manipulator model. In: Ceccarelli, M., Glazunov, V.A. (eds.) Advances on Theory and Practice of Robots and Manipulators. MMS, vol. 22, pp. 73–81. Springer, Cham (2014). https://doi.org/10.1007/978-3-319-07058-2_9
15. Pfeiffer, F., Hölzl, J.: Parameter identification for industrial robots. In: Proceedings of 1995 IEEE International Conference on Robotics and Automation, pp. 1468–1476. IEEE (1995)
16. Roesch, O.: Model-based on-line compensation of path deviations for milling robots. AMR **769**, 255–262 (2013). https://doi.org/10.4028/www.scien-tific.net/AMR.769.255
17. Timošenko, S.P., Goodier, J.N.: Theory of elasticity, 3rd edn. Engineering societies monographs. McGraw-Hill, New York (1951)
18. Mikeš, K., Jirásek, M.: Free warping analysis and numerical implementation. AMM **825**, 141–148 (2016). https://doi.org/10.4028/www.scien-tific.net/AMM.825.141